energies

MDPI

Article

Application the SBAS/EGNOS Corrections in UAV Positioning

Kamil Krasuski [1] and Damian Wierzbicki [2,*]

[1] Institute of Navigation, Military University of Aviation, 08-521 Dęblin, Poland; k.krasuski@law.mil.pl
[2] Institute of Geospatial Engineering and Geodesy, Faculty of Civil Engineering and Geodesy, Military University of Technology, 00-908 Warsaw, Poland
* Correspondence: damian.wierzbicki@wat.edu.pl; Tel.: +48-261-83-96-92

Abstract: The paper presents a new concept of determining the resultant position of a UAV (Unmanned Aerial Vehicle) based on individual SBAS (Satellite-Based Augmentation System) determinations from all available EGNOS (European Geostationary Navigation Overlay Service) satellites for the SPP (Single Point Positioning) code method. To achieve this, the authors propose a weighted mean model to integrate EGNOS data. The weighted model was based on the inverse of the square of the mean position error along the component axes of the BLh ellipsoidal frame. The calculations included navigation data from the EGNOS S123, S126, S136 satellites. In turn, the resultant UAV position model was determined using the Scilab v.6.0.0 software. Based on the proposed computational strategy, the mean values of the UAV BLh coordinates' standard deviation were better than 0.2 m (e.g., 0.0000018° = 0.01″ in angular measurement). Additionally, the numerical solution used made it possible to increase the UAV's position accuracy by about 29% for Latitude, 46% for Longitude and 72% for ellipsoidal height compared to the standard SPP positioning in the GPS receiver. It is also worth noting that the standard deviation of the UAV position calculated from the weighted mean model improved by about 21 ÷ 50% compared to the arithmetic mean model's solution. It can be concluded that the proposed research method allows for a significant improvement in the accuracy of UAV positioning with the use of EGNOS augmentation systems.

Keywords: outdoor navigation; Global Navigation Satellite System (GNSS); UAV; EGNOS; standard deviation

Citation: Krasuski, K.; Wierzbicki, D. Application the SBAS/EGNOS Corrections in UAV Positioning. *Energies* **2021**, *14*, 739. https://doi.org/10.3390/en14030739

Academic Editor: Jae-Young Pyun
Received: 30 December 2020
Accepted: 27 January 2021
Published: 31 January 2021

1. Introduction

The intensive development of unmanned aerial vehicle technologies has led to them being used in many modern technology areas. One such application is low-altitude imaging for photogrammetric and remote sensing studies. Relatively low costs of procurement and operation made this technology extremely popular [1,2]. However, still up to this day, there are UAVs (Unmanned Aerial Vehicles) available on the market that are equipped with single-frequency GPS (Global Positioning System) receivers, which allow the UAV's position to be determined with an accuracy of only just better than 10 m [3,4]. Moreover, in most of the currently available photogrammetric platforms, the UAVs use GPS pseudorange measurements in the Single Point Positioning (SPP) mode to determine the trajectory for photogrammetric studies [5]. The SPP positioning mode is the basic solution in air navigation for low-cost UAVs. The SPP method uses the L1-C/A code measurements in conjunction with data provided in the navigation message broadcast. Based on the onboard ephemeris, it is possible to calculate the satellites' coordinates, the corrections of the satellite clocks, the ionospheric correction, the relativistic correction, etc. [6]. The satellite position was estimated using the model of Keplerian orbit. In addition the clock bias is modelled using 2nd-degree polynomial model based on broadcast data. Finally, ionosphere correction is evaluated using the Klobuchar model for broadcast data [7]. It is the low-cost method of determining the position in real-time with an accuracy limited to a few meters. A significant advantage of this method is that it is used in every GNSS (Global

Navigation Satellite System) receiver installed onboard a UAV. In the SPP method, the atmospheric errors are reduced using appropriate models, while the position coordinates and the receiver clock error are determined in stochastic processing [8]. Although the SPP method is implemented in every GNSS receiver, photogrammetric applications also require the raw GNSS data converted to RINEX (Receiver Independent Exchange Format). Examples of such low-cost receivers often installed in UAVs are the uBlox 6T, uBlox M8T or NVS NV08C-CSM. The advantage of these inexpensive GNSS receivers is that they support SBAS (Satellite-Based Augmentation System) corrections on the L1 frequency [9,10]. SBAS corrections improve the SPP position's accuracy thanks to the use of fast and long-term correction models and an improved ionosphere model [11]. For example, uBlox specifies the horizontal SPP solution's achievable accuracy as 2.5 m and the accuracy with SBAS corrections as 2 m [12].

In Europe, the SBAS solution in the SPP method for UAV positioning is implemented using the EGNOS (European Geostationary Navigation Overlay Service) augmentation system. The EGNOS system increases the positioning accuracy of the UAV up to even $\pm$ 3 m [13]. That is confirmed by the latest research results on positioning using the GPS/EGNOS solution [14–16]. The conducted tests showed that a single GPS receiver's horizontal accuracy with the EGNOS function is in the range of 0.5–2.5 m, and the vertical accuracy: 1.5–3.0 m [14–16]. The current results regarding positioning assistance using the EGNOS system are included in [17]. The positioning accuracy in this document is specified as 3 m (95%) horizontally and 4 m (95%) vertically. It should be emphasized that these values are established for the entire EGNOS area.

The structure of the paper was divided into seven sections. Section 1 presents the paper introduction. Section 2 presents related works. Section 3 describes the methodology, the full algorithm of a positioning method. Section 4 elaborates the research test and scientific experiment in details. The research results from the experiment were shown in Section 6. Section 7 presents the discussion for obtained results and comparison with other solutions. The article ends with conclusions and reference list.

2. Related Works

Unmanned aerial vehicles have a wide range of applications both on the civil and military market. The demand for UAV technology is continuously growing, both in the context of performing air operations within visual line of sight (VLOS) and beyond visual line of sight (BVLOS). In Europe, the initiative of unified European airspace is referred to as U-Space. It includes the regulatory and technical framework for the gradual extension of the UAV's operability to shared airspace, also based on the Unmanned Aerial Systems (UTM) Traffic Management system. In this context, EGNOS and Galileo's use is the main chance to improve UAV navigation quality with regard to the integrity and accuracy of the positioning [18].

Currently, about 80% of GNSS receivers on the market, even the low-cost ones (including autopilot systems for UAVs), can receive corrections from SBAS systems [9,19]. The EGNOS corrections transmitted via the signal on the L1 band are beneficial to saving the battery power of the UAV and extending its flight time, as it enables the improvement of the accuracy of its position determination without additional communication channels and receiving corrections from the ground control system. It also increases the simplicity of system configuration.

Information from EGNOS is the basis for separation from other aircraft and will also play an essential role for UAVs in the future when they are integrated into civilian airspace. As mentioned before, during beyond visual line of sight (BVLOS) flights, it will be possible to detect and avoid other aircraft in a timely and appropriate manner. Moreover, thanks to information from the EGNOS system, it will be possible to increase this type of operation's security. Finally, EGNOS can also help to improve the safety functions of pilotage. This concept aims to use geographic data to establish flight boundary zones to prevent unsafe UAVS flights in sensitive areas. That can be used to restrict flights close to airfields or

above certain altitudes. A navigation solution for positioning based on EGNOS provides the means to determine whether the UAV is crossing a defined boundary zone by assessing the calculated position and the level of certainty [20]. Positioning information is expected to play a key role in achieving the ultimate goal, which is the full inclusion of UAVs in the airspace, and SBAS is by far the best, easiest and most realistic way to achieve this [9]. Currently, there are many UAVs on the market equipped with GNSS modules that support SBAS [21,22].

Much research has also been done into incorporating EGNOS information into low-altitude imaging. In studies on the acquisition of multispectral imagery from low altitudes [23], taking into account corrections from the EGNOS system made it possible to achieve a sub-meter accuracy of registration of the approximate exterior orientation elements (EOE). However, in study [24], a GNSS sensor assisted by EGNOS was used to increase the accuracy of recording thermal imagery's position from a low altitude.

An interesting application of the SBAS system in UAV technology is the support of the SAR (Search And Rescue) system. The works [25–27] show the SBAS system's use as part of the SoL (Safety of Life) service. The SoL service in the EGNOS system is designed to offer an air navigation safety service by aircraft. In the context of the use of UAV technology, this service is to improve the safety of air operations.

The work [28] shows the results of research on using the EGNOS SISNET system for precise positioning of UAVs in Poland. The tests were carried out in real-time and in the post-processing mode. The work also uses a network of GNSS reference stations located in Poland to determine the actual UAV flight trajectory.

The papers [29,30] describe the SBAS system's use in UAV positioning during the landing approach procedure. Analyzing in detail, the work [29] shows the use of SBAS corrections for UAV positioning in the absence of data from the GBAS support system. However, in [30] a model of the GNSS / SBAS approach without using ILS (Instrument landing system) was presented.

An interesting navigation solution was shown in [31], where the UAV flight trajectory was determined, and position errors in the horizontal plane of the flight were determined. The GPS / SBAS solution was included in the calculations. It should be emphasized that the research was conducted based on the PBN (Performance-Based Navigation) concept for UAV positioning.

This study aims to propose a new UAV position solution using EGNOS corrections. The solution used is based on a weighted mean model that considers a single GPS/EGNOS position solution from satellites S123, S126 and S136. The numerical solution's construction uses the weighting of the measurements as a function of the inverse of the square of the mean error of the UAV coordinates in the BLh ellipsoidal frame. Moreover, the proposed numerical solution enables the analysis of the accuracy of the determined resultant UAV coordinates. Such a position model is characterized by a uniform influence of the particular GPS/EGNOS solution on the resultant UAV coordinates. Therefore, it can be concluded that the use of the GPS/EGNOS solution from satellites S123, S126 and S136 causes the resultant UAV coordinates to be defined for the number of degrees of freedom equal to 2.

Finally, the research contributions are focused on:

1. Presenting the new positioning model using EGNOS corrections from 3 satellites, e.g., S123, S126, S136;
2. Integration the SBAS corrections in the weighted mean algorithm;
3. Improving the accuracy of UAV positioning using multiple EGNOS solution;
4. Comparison the positioning results of UAV from the weighted mean model and average mean model.

3. Research Method

The process of determining the impact of the corrections from several EGNOS satellites on the determination of the UAV's position is carried out in two stages. EGNOS corrections are used to improve the accuracy performance of GPS navigation positioning. In the

first stage, the methodology describing the mathematical model's scheme using EGNOS corrections from one SBAS satellite will be presented. Next, the second diagram will present the methodology for determining the UAV position based on the GPS solution with the use of corrections from several SBAS satellites. In addition, for the second stage of calculations, analysis of the EGNOS positioning accuracy for UAVs will also be presented.

3.1. Designation the UAV Position Based on a Single GPS+EGNOS Solution

The methodology of the first stage is based on the implementation of EGNOS corrections from one SBAS satellite to the mathematical model of GPS positioning in aviation, as presented below [32,33]:

$$l = d_{GPS/EGNOS} + c\cdot(dtr - dts_{GPS/EGNOS}) + Ion_{EGNOS} + Trop_{EGNOS} + Rel + TGD + Mp \quad (1)$$

where: l—code measurements in the GPS receiver, $d_{GPS/EGNOS}$—geometric distance satellite-receiver, the long-term and fast EGNOS corrections are applied for designation the geometric distance satellite-receiver, $d_{GPS/EGNOS} = \sqrt{(X - X_{GPS/EGNOS})^2 + (Y - Y_{GPS/EGNOS})^2 + (Z - Z_{GPS/EGNOS})^2}$; (X, Y, Z)–geocentric coordinates of UAV vehicle; $X_{GPS/EGNOS} = Xs_{GPS} + \delta x_{EGNOS}$, GPS satellite coordinate along the X axis, $Y_{GPS/EGNOS} = Ys_{GPS} + \delta y_{EGNOS}$, GPS satellite coordinate along the Y axis, $Z_{GPS/EGNOS} = Zs_{GPS} + \delta z_{EGNOS}$, GPS satellite coordinate along the Z axis, $(Xs_{GPS}, Ys_{GPS}, Zs_{GPS})$—GPS coordinates based on ephemeris data, $(\delta x_{EGNOS}, \delta y_{EGNOS}, \delta_{EGNOS})$—the long-term and fast EGNOS corrections, c—the speed of light, dtr—receiver clock bias, $dts_{GPS/EGNOS}$—satellite clock bias, the long-term and fast EGNOS corrections are applied for designation the satellite clock bias, $dts_{GPS/EGNOS} = dts_{GPS} + \delta dts_{EGNOS}$, dts_{GPS}—satellite clock bias based on ephemeris data, δdts_{EGNOS}—the long-term and fast EGNOS corrections, Ion_{EGNOS}—ionosphere correction, based on SBAS ionosphere model, $Ion_{EGNOS} = MF\cdot\sum w_n\cdot VTEC_n$, MF—mapping function, w_n—weight, the function of the distance between GRID coordinates in each node and current ionosphere pierce point coordinates, $VTEC_n$—Vertical TEC at each node of GRID coordinates, $Trop_{EGNOS}$—troposphere correction, based on RTCA-MOPS model, $Trop_{EGNOS} = \frac{1.001}{\sqrt{0.002001 + sin^2 El}}\cdot(ZHD_{SBAS} + ZWD_{SBAS})$, $ZHD_{SBAS} = ZHD_0\cdot\left(1 - \frac{\beta\cdot h}{T_K}\right)^{\frac{g}{R_d\cdot\beta}}$, $ZWD_0\cdot\left(1 - \frac{\beta\cdot h}{T_K}\right)^{\frac{g\cdot(\lambda+1)}{R_d\cdot\beta} - 1}$, (ZHD_0, ZWD_0)—ZHD and ZWD term at sea level, (λ, β)—water vapour lapse rate and temperature lapse rate, (g, R_d)—constant coefficients, h—ellipsoidal height, T_K—temperature, El—elevation angle, Rel—relativistic effect in the GPS receiver, TGD—Timing Group Delay for GPS satellite, Mp—multipath effect in the GPS receiver.

Based on Equation (1), the UAV coordinates are determined in the GNSS navigation system based on a single GPS+EGNOS solution using the least-squares method [34,35], such as below:

$$\begin{cases} \begin{cases} Q_X = N^{-1}\cdot L \\ v = A\cdot Q_X - dl \end{cases} \\ m0_{post} = \sqrt{\frac{[v^T pv]}{n-k}} \end{cases} \quad \begin{cases} C_{Qx} = m0^2_{post}\cdot N^{-1} \\ m_{Qx} = diag\left(\sqrt{C_{Qx}}\right) \end{cases} \quad (2)$$

where: Q_X—vector with unknown parameters, $N = A^T\cdot p\cdot A$—matrix of normal equation frame, A—matrix of plan, v—residuals vector, p—matrix of weights, $p = \frac{1}{m0^2\cdot ml^2}$, $m0$—unit mean error a priori, $m0 = 1$, ml—pseudorange measurement error matrix, $ml = \sqrt{\left(\frac{ml_0}{\sin(El)}\right)^2 + m^2_{SBAS/EGNOS}}$—mean error of pseudorange, ml_0—mean error of pseudorange in GPS system, $ml_0 = 1\ m$, $m_{SBAS/EGNOS}$—mean error of SBAS correction model, $L = A^T\cdot p\cdot dl$—vector of absolute terms, dl—vector with difference between measurements and modeled parameters, $m0_{post}$—unit mean error a posteriori, n—number of observations for each measurement epoch, k—number of unknown parameters for each measurement

epoch, C_{Qx}—variance-covariance matrix in XYZ coordinates, m_{Qx}—mean errors of XYZ coordinates of UAV.

The position of the UAV is determined with a specific time interval, usually every 1 s. In the observation Equation (1), EGNOS corrections for ephemeris data and GPS satellite clocks, ionospheric and tropospheric delay are applied. The obtained position based on Equation (2) is referenced to XYZ coordinates. In addition, the UAV position is better determined in aerial navigation in ellipsoidal coordinates BLh (B-Latitude, L-Longitude, h-ellipsoidal height). The position of the UAV in BLh ellipsoidal coordinates is described as follows [35]:

$$\begin{bmatrix} B \\ L \\ h \end{bmatrix} = \begin{bmatrix} \arctan\left(\frac{Z}{\rho} + \frac{\delta_1 \cdot tgB_{i-1}}{\sqrt{\delta_2 \cdot tg^2 B_{i-1}}}\right) \\ \arctan\left(\frac{Y}{X}\right) \\ \frac{\rho}{cosB} - R \end{bmatrix} \tag{3}$$

where: (a, b)—ellipsoid semi-major axis and semi-minor axis, e—first flattening, $e = \sqrt{\frac{a^2-b^2}{a^2}}$, R—radius of the curvature in the prime vertical, $R = \frac{1}{\sqrt{1-e^2 \cdot sin^2 B}}$, $\rho = \sqrt{X^2 + Y^2}$, $\delta_1 = \frac{a \cdot e}{\rho \cdot \sqrt{1-e^2}}$, $\delta_2 = \frac{1}{1-e^2}$, $i-1$—previous iteration, (B, L, h)—UAV ellipsoidal coordinates, B—geodetic Latitude, L—geodetic Longitude, h—ellipsoidal height.

The mean error values m_{Qx} of the calculated geocentric XYZ coordinates for the UAV may also be expressed in the BLh ellipsoidal coordinate frame, as shown below [36,37]:

$$\begin{bmatrix} mB \\ mL \\ mh \end{bmatrix} = \begin{bmatrix} \sqrt{m_{BLh}(1,1)} \\ \sqrt{m_{BLh}(2,2)} \\ \sqrt{m_{BLh}(3,3)} \end{bmatrix} \tag{4}$$

where: m_{BLh}—variance-covariance matrix of parameters in the BLh ellipsoidal frame, $m_{BLh} = R \cdot C_{Qx} \cdot R^T$, R—conversion matrix from the XYZ geocentric frame to the BLh geodetic frame, mB—mean error for geodetic latitude B, mL—mean error for geodetic longitude L, mh—mean error for ellipsoidal height h.

The calculated position of the UAV in the form of BLh coordinates and their mean errors (mB, mL, mh) will be used for the next stage of the research. It should be noted that Equations (1)–(4) denote an algorithm for determining the UAV position for GPS positioning using SBAS corrections from a single EGNOS satellite. Therefore, it can be said that the Equations (1)–(4) is a single GPS + EGNOS solution in UAV positioning.

3.2. Designation the UAV Position Based on GPS+EGNOS Solution

The second stage methodology is based on the GPS+EGNOS position navigation solution with corrections from several SBAS satellites, as presented below:

$$\begin{cases} B^m_{GPS/EGNOS} = \frac{pB_{GPS/S123} \cdot B^i_{GPS/S123} + pB_{GPS/S126} \cdot B^j_{GPS/S126} + pB_{GPS/S136} \cdot B^k_{GPS/S136}}{pB_{GPS/S123} + pB_{GPS/S126} + pB_{GPS/S136}} \\ L^m_{GPS/EGNOS} = \frac{pL_{GPS/S123} \cdot L^i_{GPS/S123} + pL_{GPS/S126} \cdot L^j_{GPS/S126} + pL_{GPS/S136} \cdot L^k_{GPS/S136}}{pL_{GPS/S123} + pL_{GPS/S126} + pL_{GPS/S136}} \\ h^m_{GPS/EGNOS} = \frac{ph_{GPS/S123} \cdot h^i_{GPS/S123} + ph_{GPS/S126} \cdot h^j_{GPS/S126} + ph_{GPS/S136} \cdot h^k_{GPS/S136}}{ph_{GPS/S123} + ph_{GPS/S126} + ph_{GPS/S136}} \end{cases} \tag{5}$$

where: $\left(B^m_{GPS/EGNOS}, L^m_{GPS/EGNOS}, h^m_{GPS/EGNOS}\right)$—resultant UAV position, overall weighted mean based on a GPS+EGNOS position navigation solution with corrections from several SBAS satellites, (i, j, k)—solution index, $(i = j = k) = 1$, $(pB_{GPS/S123}, pB_{GPS/S126}, pB_{GPS/S136})$—measurement weights along the B axis for a single GPS + EGNOS solution, $(pL_{GPS/S123}, pL_{GPS/S126}, pL_{GPS/S136})$—measurement weights along the L axis for a single GPS + EGNOS solution, $(ph_{GPS/S123}, ph_{GPS/S126}, ph_{GPS/S136})$—measurement weights along the h axis for a single GPS + EGNOS solution, $(S123, S126, S136)$—index of the EGNOS satellite, $(B^i_{GPS/S123}, L^i_{GPS/S123}, h^i_{GPS/S123})$—UAV position determined from a single GPS+EGNOS solution using corrections from satellite S123, $(B^j_{GPS/S126}, L^j_{GPS/S126}, h^j_{GPS/S126})$

—UAV position determined from a single GPS+EGNOS solution using corrections from the S126 satellite, $(B^k_{GPS/S136}, L^k_{GPS/S136}, h^k_{GPS/S136})$—UAV position determined from a single GPS+EGNOS solution using corrections from the S136 satellite.

Mathematical Equation (5) provides a weighted mean model to determine the resultant UAV position based on the EGNOS corrections from several SBAS satellites. The mathematical model in Equation (5) is based on the application of EGNOS corrections from SBAS satellites S123, S126 and S136.

The measurement weights were defined as the inverse of the squared mean error values of the determined coordinates as below:

$$\begin{cases} pB_{GPS/S123} = \frac{1}{mB^2_{GPS/S123}} \\ pB_{GPS/S126} = \frac{1}{mB^2_{GPS/S126}} \\ pB_{GPS/S136} = \frac{1}{mB^2_{GPS/S136}} \\ pL_{GPS/S123} = \frac{1}{mL^2_{GPS/S123}} \\ pL_{GPS/S126} = \frac{1}{mL^2_{GPS/S126}} \\ pL_{GPS/S136} = \frac{1}{mL^2_{GPS/S136}} \\ ph_{GPS/S123} = \frac{1}{mh^2_{GPS/S123}} \\ ph_{GPS/S126} = \frac{1}{mh^2_{GPS/S126}} \\ ph_{GPS/S136} = \frac{1}{mh^2_{GPS/S136}} \end{cases} \quad (6)$$

where: $(mB_{GPS/S123}, mL_{GPS/S123}, mh_{GPS/S123})$—mean error values of the UAV coordinates determined using the EGNOS corrections from satellite S123, $(mB_{GPS/S126}, mL_{GPS/S126}, mh_{GPS/S126})$—mean error values of the UAV coordinates determined using the EGNOS corrections from satellite S126, $(mB_{GPS/S136}, mL_{GPS/S136}, mh_{GPS/S136})$—mean error values of the UAV coordinates determined using the EGNOS corrections from satellite S136.

Taking into account the measuring weights in Equation (5), we obtain:

$$\begin{cases} B^m_{GPS/EGNOS} = \frac{\frac{1}{mB^2_{GPS/S123}} \cdot B^i_{GPS/S123} + \frac{1}{mB^2_{GPS/S126}} \cdot B^j_{GPS/S126} + \frac{1}{mB^2_{GPS/S136}} \cdot B^k_{GPS/S136}}{\frac{1}{mB^2_{GPS/S123}} + \frac{1}{mB^2_{GPS/S126}} + \frac{1}{mB^2_{GPS/S136}}} \\ L^m_{GPS/EGNOS} = \frac{\frac{1}{mL^2_{GPS/S123}} \cdot L^i_{GPS/S123} + \frac{1}{mL^2_{GPS/S126}} \cdot L^j_{GPS/S126} + \frac{1}{mL^2_{GPS/S136}} \cdot L^k_{GPS/S136}}{\frac{1}{mL^2_{GPS/S123}} + \frac{1}{mL^2_{GPS/S126}} + \frac{1}{mL^2_{GPS/S136}}} \\ h^m_{GPS/EGNOS} = \frac{\frac{1}{mh^2_{GPS/S123}} \cdot h^i_{GPS/S123} + \frac{1}{mh^2_{GPS/S126}} \cdot h^j_{GPS/S126} + \frac{1}{mh^2_{GPS/S136}} \cdot h^k_{GPS/S136}}{\frac{1}{mh^2_{GPS/S123}} + \frac{1}{mh^2_{GPS/S126}} + \frac{1}{mh^2_{GPS/S136}}} \end{cases} \quad (7)$$

For the $(B^m_{GPS/EGNOS}, L^m_{GPS/EGNOS}, h^m_{GPS/EGNOS})$ parameters, the values of the standard deviation are determined as follows:

$$\begin{cases} \delta B = \sqrt{\frac{pB_{GPS/S123} \cdot v^2_{B,i} + pB_{GPS/S126} \cdot v^2_{B,j} + pB_{GPS/S136} \cdot v^2_{B,k}}{ns-1}} \\ \delta L = \sqrt{\frac{pL_{GPS/S123} \cdot v^2_{L,i} + pL_{GPS/S126} \cdot v^2_{L,j} + pL_{GPS/S136} \cdot v^2_{L,k}}{ns-1}} \\ \delta h = \sqrt{\frac{ph_{GPS/S123} \cdot v^2_{h,i} + ph_{GPS/S126} \cdot v^2_{h,j} + ph_{GPS/S136} \cdot v^2_{h,k}}{ns-1}} \end{cases} \quad (8)$$

where: $(v_{B,i}, v_{B,j}, v_{B,k})$—residuals along the B axis, $v_{B,i} = B^i_{GPS/S123} - B^m_{GPS/EGNOS}$, $B^j_{GPS/S126} - B^m_{GPS/EGNOS}$, $v_{B,k} = B^k_{GPS/S136} - B^m_{GPS/EGNOS}$, $(v_{L,i}, v_{L,j}, v_{L,k})$—residuals along the L axis, $v_{L,i} = L^i_{GPS/S123} - L^m_{GPS/EGNOS}$, $v_{L,j} = L^j_{GPS/S126} - L^m_{GPS/EGNOS}$, $v_{L,k} = L^k_{GPS/S136} - L^m_{GPS/EGNOS}$, $\left(v_{h,i}, v_{h,j}, v_{h,k}\right)$—residuals along the h axis, $v_{h,i} = h^i_{GPS/S123} - h^m_{GPS/EGNOS}$,

$v_{h,j} = h^j_{GPS/S126} - h^m_{GPS/EGNOS}$, $v_{h,k} = h^k_{GPS/S136} - h^m_{GPS/EGNOS}$, $ns = 3$ for each measurement epoch.

In general notation, Equations (5), (7) and (8) can be simplified to the form:

- to determine the resultant position of the UAV:

$$\begin{cases} B^m_{GPS/EGNOS} = \frac{\sum_1^3 pB_s \cdot B_s}{\sum_1^3 pB_s} \\ L^m_{GPS/EGNOS} = \frac{\sum_1^3 pL_s \cdot L_s}{\sum_1^3 pL_s} \\ h^m_{GPS/EGNOS} = \frac{\sum_1^3 ph_s \cdot h_s}{\sum_1^3 ph_s} \end{cases} \quad (9)$$

$$\begin{cases} B^m_{GPS/EGNOS} = \frac{\sum_1^3 \frac{1}{mB_s^2} \cdot B_s}{\sum_1^3 \frac{1}{mB_s^2}} \\ L^m_{GPS/EGNOS} = \frac{\sum_1^3 \frac{1}{mL_s^2} \cdot L_s}{\sum_1^3 \frac{1}{mL_s^2}} \\ h^m_{GPS/EGNOS} = \frac{\sum_1^3 \frac{1}{mh_s^2} \cdot h_s}{\sum_1^3 \frac{1}{mh_s^2}} \end{cases} \quad (10)$$

- to determine the standard deviation of the individual components of the resultant position of the UAV:

$$\begin{cases} \delta B = \sqrt{\frac{\sum_1^3 pB_s \cdot v^2_{B,s}}{ns-1}} \\ \delta L = \sqrt{\frac{\sum_1^3 pL_s \cdot v^2_{L,s}}{ns-1}} \\ \delta h = \sqrt{\frac{\sum_1^3 ph_s \cdot v^2_{h,s}}{ns-1}} \end{cases} \quad (11)$$

where: s–index of solution GPS/S123, GPS/S126, GPS/S136.

3.3. Accuracy Analysis of the GPS + EGNOS Solution

The accuracy analysis of the presented research method is based on a three-step calculation scheme, as shown below:

(I) establishing UAV position errors determined as absolute values from the comparison between the resultant GPS+EGNOS solution and the reference position calculated by the RTK differential technique [38]:

$$\begin{cases} DB = B^m_{GPS/EGNOS} - B_{RTK} \\ DL = L^m_{GPS/EGNOS} - L_{RTK} \\ Dh = h^m_{GPS/EGNOS} - h_{RTK} \end{cases} \quad (12)$$

(II) establishing statistical accuracy in the form of the RMS error [39]:

$$\begin{cases} RMS_{DB} = \sqrt{\frac{[DB^2]}{N}} \\ RMS_{DL} = \sqrt{\frac{[DL^2]}{N}} \\ RMS_{Dh} = \sqrt{\frac{[Dh^2]}{N}} \end{cases} \quad (13)$$

(III) establishing the mean absolute error:

$$\begin{cases} \overline{DB} = \frac{\sum|DB|}{N} \\ \overline{DL} = \frac{\sum|DL|}{N} \\ \overline{Dh} = \frac{\sum|Dh|}{N} \end{cases} \quad (14)$$

where: (DB, DL, Dh)—position error based on the GPS + EGNOS solution, $(B_{RTK}, L_{RTK}, h_{RTK})$—reference position of the UAV, based on RTK solution, $(RMS_{DB}, RMS_{DL}, RMS_{Dh})$—RMS errors along the BLh axis based on the GPS + EGNOS solution, $\left(\overline{DB}, \overline{DL}, \overline{Dh}\right)$—absolute error based on the GPS + EGNOS solution, N—all measurement epochs.

In the first stage of the accuracy analysis, the UAV position errors are calculated as the difference between the resultant GPS + EGNOS solution and the RTK differential method. RMS errors are determined sequentially, which are a statistical measure of accuracy along each BLh axis. Additionally, the accuracy analysis also includes the calculation of the absolute error along each BLh axis.

The mathematical scheme (12)–(14) presented the comparison between multiple GPS+EGNOS solutions and the RTK reference trajectory. This approach is used to determine the UAV position's accuracy in reference to the RTK measurement technique. During the flight, the UAV position was estimated using the SPP GPS solution as a basic positioning model of the flight trajectory. It is necessary to calculate the difference between the multiple GPS+EGNOS solutions and the SPP GPS real model of the UAV's trajectory. It should be evaluated as below [40]:

$$\begin{cases} rB = B^m_{GPS/EGNOS} - B_{SPP,real} \\ rL = L^m_{GPS/EGNOS} - L_{SPP,real} \\ rh = h^m_{GPS/EGNOS} - h_{SPP,real} \end{cases} \quad (15)$$

where: (rB, rL, rh)—difference between the multiple GPS+EGNOS solution and the real UAV trajectory from the SPP GPS model, $(B_{SPP,real}, L_{SPP,real}, h_{SPP,real})$—UAV trajectory from the SPP GPS model.

Equation (15) shows the convergence between the multiple GPS+EGNOS solution and the UAV trajectory from the SPP GPS model. It is a good indicator in navigational analyses of the obtained UAV position.

4. Research Test

As part of the research analysis, the GNSS data recorded by an AsteRx-m2 UAS receiver placed on the Tailsitter unmanned platform was used. The flying platform was equipped with a single-frequency GNSS receiver, recording data at a frequency of 10 Hz. The Tailsitter platform is a type of VTOL aircraft. The general characteristics of the UAV platform include: capacity: 800 g payload, wingspan: 1.25 m, empty weight: 3.6 kg, max takeoff weight: 4.4 kg. The Tailsitter platform model is presented in Figure 1.

Figure 1. The Tailsitter unmanned ariel vehicle (UAV) model before flight start.

The UAV platform performed a photogrammetric flight in south-eastern Poland. GNSS navigation data was acquired on 23 April 2020, between 11:00 a.m.—2:00 p.m. local time. The temperature was 17 °C, while the wind speed was around 2 m/s. Figure 2 shows the UAV flight trajectory in the ellipsoidal coordinate frame BL (B—geodetic Latitude, L-geodetic Longitude). The flight trajectory in Figure 2 is the resultant of the UAV position for horizontal coordinates, calculated according to Equation(7). The minimum value of B component equals 50.499204°, whereas the maximum values were about 50.512818°. The

minimum value of L coordinate equals 20.655142°, whereas the maximum values were about 20.703802°, respectively. The difference of range the Latitude equals to 0.013614° and difference of range the Longitude equals to 0.04866°.

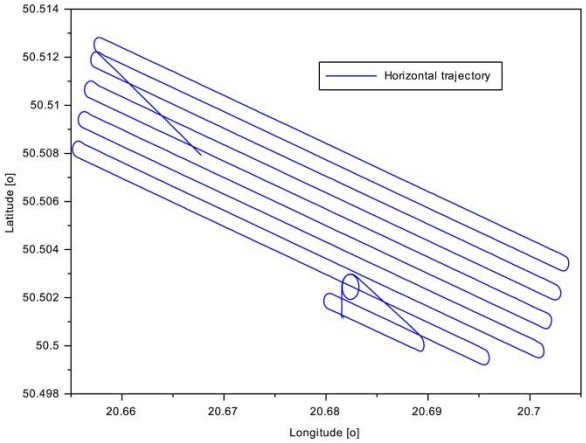

Figure 2. The horizontal trajectory of the UAV.

The maximum flight altitude was approximately 250 m relative to the height of the route starting point. Figure 3 shows the UAV flight's vertical trajectory as a function of time when the position was recorded. The flight trajectory in Figure 3 is the resultant UAV position for the vertical component, calculated by the Equation (7). The h component changed during the flight from 296.87 to 545.12 m.

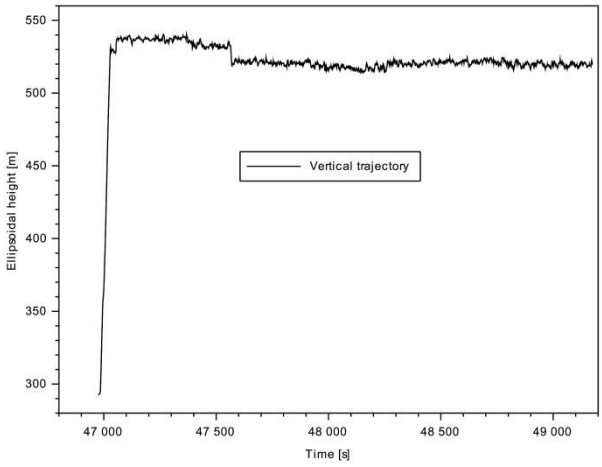

Figure 3. The vertical trajectory of the UAV.

The experiment was carried out from 13:02:56 to 13:39:35 according to GPS Time. It was, therefore, necessary to determine the state of the ionosphere during the UAV flight. The VTEC parameter was used to determine the ionosphere's state, which was then determined based on the SBAS ionosphere model. The VTEC parameter values are determined for EGNOS corrections from tracked and available SBAS satellites PRN S123, S126 and S136. The free SBAS Mentor v.1.15 software was used to perform the calculations [41]. Table 1 shows the results of the VTEC parameter. Based on the EGNOS corrections, it was found that the VTEC values for satellites S123, S126 and S136 are the same and amounted to 1.375 m during the research test. Moreover, Table 1 presents the GIVE parameter index values, which was constant during the research test and was equal to 8.

Table 1. The value of VTEC for SBAS ionosphere model.

Time [s]	VTEC (S123) (m)	VTEC (S126) (m)	VTEC (S136) (m)
13:02:56	1.375	1.375	1.375
13:39:35	1.375	1.375	1.375
Time [s]	**GIVE Index (S123)**	**GIVE Index (S126)**	**GIVE Index (S136)**
13:02:56	8	8	8
13:39:35	8	8	8

In the first phase of the test, the UAV position calculations were performed in the RTKPOST library of the RTKLIB program (see Equation (1)). Therefore, in the RTKPOST application, the configuration was set as follows [42,43]:

- Positioning mode: Single (Single Point Positioning);
- Elevation mask: 5°;
- Input data: RINEX NAV GPS, RINEX OBS GPS, EMS FILE;
- EMS file: SBAS123, SBAS126, SBAS 136;
- Source of ionosphere correction: SBAS model;
- Source of troposphere correction: SBAS model;
- Source of ephemeris data/clock: Broadcast ephemeris + SBAS;
- Output coordinates: BLh ellipsoidal;
- Interval of computations: 1 s.

The obtained results of the UAV positions from the RTKLIB program were used for further analysis of the research. At this stage, calculations are performed with the use of proprietary numerical scripts in the Scilab 6.0.0 language environment [44]. The mathematical analysis of calculations in Scilab applies to Equations (2)–(7). The test and simulation results are presented in Section 5.

5. Results

The EGNOS positioning concept assumes that the corrections from SBAS satellites should be identical. However, in many research studies, the problem of the quality of EGNOS corrections was noticed and analyzed. For example, in [45], the accuracy of GPS + EGNOS positioning at airfields in Poland was shown. The authors of the work pointed out that the corrections transmitted by the EGNOS satellites are different, which directly impacts the accuracy of the determined ellipsoidal BLh coordinates for the reference stations. Another work [46] shows the differences in the coordinates of three GNSS reference stations installed on the aircraft flight path. Based on the performed tests, it was found that there are quite significant differences in the XYZ coordinates of the reference stations based on the EGNOS corrections applied from satellites S120, S124 and S126 and the catalogue position of the base stations. In addition, the paper [47] presents the results of research on the application of EGNOS corrections from satellites S120, S124 and S126 in air navigation. The paper describes the differences between individual GPS + EGNOS solutions determining the position of the aircraft. Based on the research results obtained, it can be seen that the quality of EGNOS corrections significantly influenced the position of the aircraft during the test flight. Moreover, the aircraft's determined position from a particular GPS + EGNOS solution was different, which only emphasizes that the problem of the impact of EGNOS corrections on kinematic positioning in air navigation should be addressed. Therefore, this work and the proposed solution of the weighted average model may significantly influence the further development of scientific works in the context of the implementation of SBAS in aviation.

In support of the considerations on EGNOS corrections' quality in the first stage of the research, the results of the difference of the estimated BLh ellipsoidal coordinates of the UAV position between the individual GPS + EGNOS solutions were shown, in accordance with the Equation (1). Figure 4 shows the results of the B coordinate difference for the UAV position between the various GPS + EGNOS solutions. The B coordinate difference

between GPS + S123 and GPS + S126 is from −0.42 to +1.04 m, and the arithmetic mean of the difference is 0.04 m. The B coordinate difference between GPS + S123 and GPS + S136 is from −0.09 to +0.14 m, and the arithmetic mean of this difference is 0.01 m. It can be stated that solutions GPS + S123 and GPS + S136 overlap and are quite closely aligned with each other. On the other hand, the difference of the B coordinate between the solutions GPS + S126 and GPS + S136 ranges from −1.04 to +0.41 m, and the arithmetic mean of this difference is −0.03 m.

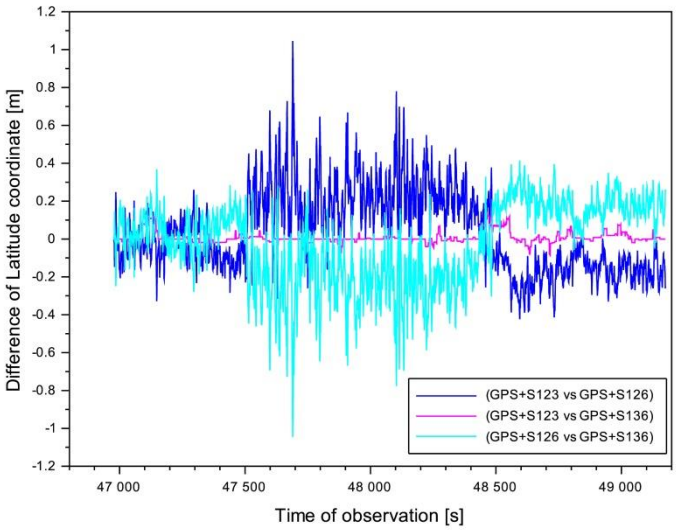

Figure 4. The difference of the Latitude coordinate of the UAV.

Figure 5 shows the results of the difference in the L coordinate for the UAV position between the various GPS + EGNOS solutions. The L-coordinate difference between GPS + S123 and GPS + S126 is from −1.83 to +0.56 m, and the arithmetic mean of this difference is −0.27 m. The L-coordinate difference between GPS + S123 and GPS + S136 is from −0.16 to +0.14 m, and the arithmetic mean of this difference is −0.01 m. In this case, it is worth noting that the solutions GPS + S123 and GPS + S136 coincide and are quite closely aligned. In turn, the difference in the L coordinate between the solutions GPS + S126 and GPS + S136 ranges from −0.65 to +1.80 m, and the arithmetic mean of this difference is +0.26 m.

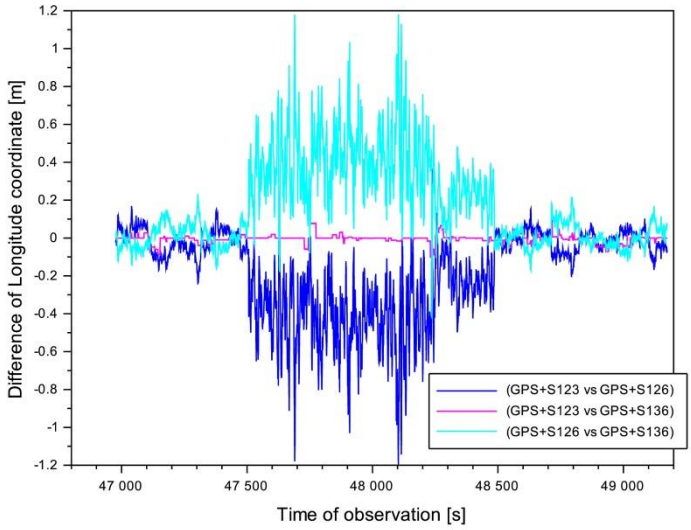

Figure 5. The difference in the Longitude coordinate of the UAV.

Figure 6 shows the results of the h coordinate difference for the UAV position between the various GPS + EGNOS solutions. The L-coordinate difference between GPS + S123 and GPS + S126 is from −2.92 to +0.60 m, and the arithmetic mean of this difference is -0.41 m. The h-coordinate difference between GPS + S123 and GPS + S136 is from −0.30 to +0.18 m, and the arithmetic mean of this difference is −0.01 m. For the h component, the results of the solutions GPS + S123 and GPS + S136 coincide and are quite convergent with each other. In turn, the difference in the h coordinate between the solutions GPS + S126 and GPS + S136 ranges from −0.75 to +2.92 m, and the arithmetic mean of this difference is +0.40 m.

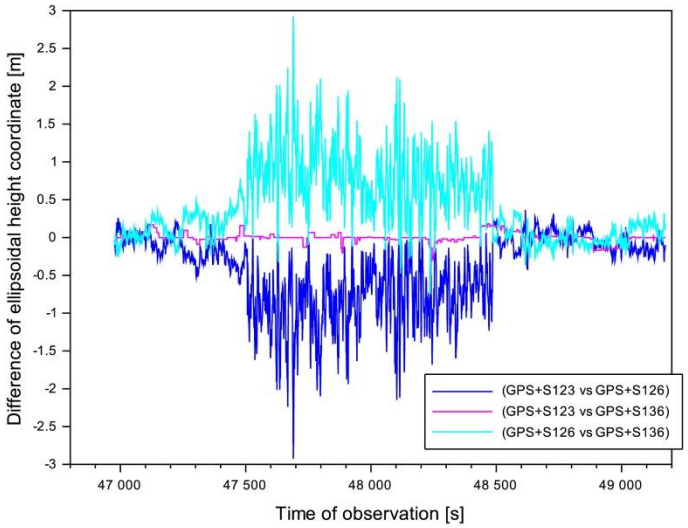

Figure 6. The difference in the ellipsoidal height coordinate of the UAV.

From the calculated BLh coordinate differences for the UAV positions, it can be seen that the EGNOS corrections transmitted by the individual satellites S123, S126, S136 are different. In particular, the difference in coordinates is significant when applying the corrections from satellite S126.

Therefore, the impact of individual corrections from EGNOS satellites on the determination of the resultant position of the UAV according to the proposed model of Equations (1)–(8) will be visible. The developed model of solving Equations (1)–(8) to determine the resultant position of the UAV is correct, assuming obtaining different values of BLh coordinates from a single GPS + EGNOS solution (see Equation (1)).

As part of the next step, Figure 7 shows the results of the standard deviation parameters $(\delta B, \delta L, \delta h)$ in the BLh ellipsoidal coordinates. The δB parameter values ranged from 0.01 to 0.62 m. Moreover, the arithmetic mean for the parameter δB is equal to 0.11 m. The δL parameter values ranged from 0.01 to 1.14 m. The arithmetic mean for the δL parameter is 0.20 m. The δh parameter values ranged from 0.01 to 0.81 m. Moreover, the arithmetic mean for the δh parameter is 0.13 m. It is worth noting that from the measuring epoch 47,500 s to 48,500 s, the $(\delta B, \delta L, \delta h)$ parameter values continue to increase up to the maximum value of 1.14 m. Ignoring this period, the $(\delta B, \delta L, \delta h)$ parameter values do not exceed 0.25 m. It should be noted that the highest values of the standard deviation are visible for the L component. The values of the standard deviation along the L axis were determined according to Equation (8). Therefore, the distribution of corrections has the most significant impact on the values of the standard deviation along the L axis $(v_{L,i}, v_{L,j}, v_{L,k})$ and the measurement weights $(pL_{GPS/S123}, pL_{GPS/S126}, pL_{GPS/S136})$. In the stochastic model, the value of the standard deviation is significantly influenced by the measurement weights compared to the model of equally accurate measurements shown in Equation (18).

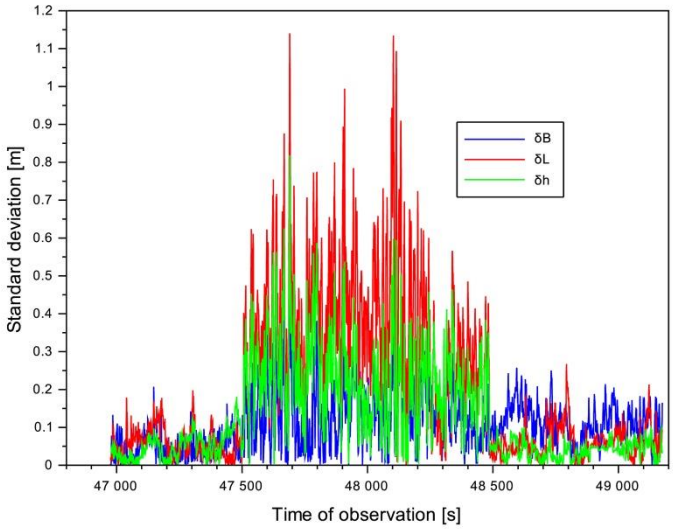

Figure 7. The results of the standard deviation of the UAV's position.

The standard deviation values along the L axis are greater than for the horizontal component B or the vertical component h.

Table 2 shows the results of the arithmetic mean for the obtained values of the proportionality coefficients (rBL, rhB, rhL). Based on the obtained results, it can be concluded that the best fit of the standard deviation values is between the h and L components. The values of the proportionality coefficients vary from 2.09 to 2.89. The proportionality coefficient is important because it determines the relations between the values of standard deviations of individual BLh components. The closer its value is to 1, the more the standard deviation's distribution is in a similar trend. The parameters (rBL, rhB, rhL) were estimated as below:

$$\begin{cases} rBL = \frac{\overline{\delta B}}{\overline{\delta L}} \\ rhB = \frac{\overline{\delta h}}{\overline{\delta B}} \\ rhL = \frac{\overline{\delta h}}{\overline{\delta L}} \end{cases} \tag{16}$$

where: $\left(\overline{\delta B}, \overline{\delta L}, \overline{\delta h}\right)$—mean value of standard deviations along to BLh axis.

Table 2. The arithmetic mean of the (rBL, rhB, rhL) coefficients.

Parameter	Coefficient rBL	Coefficient rhB	Coefficient rhL
Arithmetic Mean	2.89	2.32	2.09

The next stage of the research concerns the analysis of the UAV positioning accuracy. Figure 8 presents the position errors of UAV. In the first part of the analysis, the (DB, DL, Dh) parameters were determined in accordance with Equation (12). The position error values of the (DB, DL, Dh) parameters do not exceed the values of 2.01, 2.09 and 3.98 m, respectively.

Table 3 shows the results of the obtained accuracy parameters $(RMS_{DB}, RMS_{DL}, RMS_{Dh})$, calculated according to Equation (13). Based on the obtained results, it can be concluded that the highest accuracy is noticeable for the B component, and the lowest for the h component. The RMS parameter values are 0.92 m along the B axis, 1.08 m along the L axis and 1.42 m along the h axis. The B components RMS error values do not exceed 1 m. The RMS error values along the L and h axes do not exceed 2 m. However, it can be concluded that for the proposed research method, the accuracy of the UAV positioning along the BLh axes is relatively high.

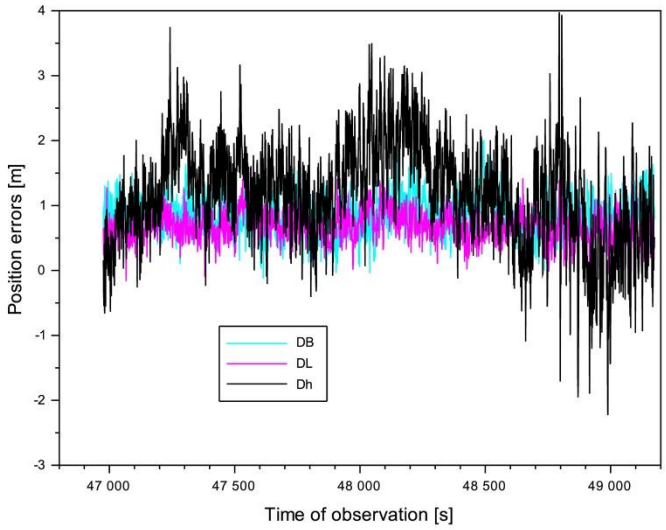

Figure 8. The results of position errors of the UAV.

Table 3. The results of the $(RMS_{DB}, RMS_{DL}, RMS_{Dh})$ parameters.

Parameter	RMS_{DB} [m]	RMS_{DL} [m]	RMS_{Dh} [m]
Value	0.92	1.08	1.59

Table 4 shows the results of the obtained mean absolute error values $\left(\overline{DB}, \overline{DL}, \overline{Dh}\right)$, calculated according to the Equation (14). Based on the obtained results, it can be concluded that the smallest absolute error results are noticeable for the B component, and the largest for the h component. The $\left(\overline{DB}, \overline{DL}, \overline{Dh}\right)$ parameter values are, respectively: 0.87 m along the B axis, 0.56 m along the L axis and 1.24 m along the h axis. The absolute error values along the L and B axes do not exceed 1 m.

Table 4. The results of $\left(\overline{DB}, \overline{DL}, \overline{Dh}\right)$ parameters.

Parameter	$\overline{DB}$ [m]	$\overline{DL}$ [m]	$\overline{Dh}$ [m]
Value	0.87	0.56	1.46

In the next step, the BLh coordinates from the GPS + EGNOS solution were compared to the actual flight trajectory from the SPP GPS model based on Equation (15). The differences in coordinates (rB, rL, rh) are shown in Figure 9. The coordinate difference ranges from -0.99 to +0.22 m for the B component, -0.46 to +1.21 m for the L component, for the h component +3,90 to 6.64 m. Based on the obtained (rB, rL, rh) results, a significant shift along the vertical axis h can be seen. The mean value of the differences in coordinates are: -0.34 m for the B coordinate, +0.47 m for the L coordinate, and 5.30 m for the h coordinate. It is worth paying attention to the numerous changes in the coordinate difference in Figure 9. The reason for this phenomenon can be found in the number of tracked GPS satellites. Thus, for the measurement epoch 47,500 s, the number of tracked GPS satellites for the SBAS123 and SBAS136 solution was 7. On the other hand, for the same moment in time from the SBAS126 solution, the number of GPS satellites changed from 8 to 9. Another jump is visible for the measurement epoch 48,500 s. Therefore, with SBAS123 and SBAS136, 8 GPS satellites are tracked, while SBAS126 changes the number of tracked GPS satellites from 10 to 9. Successive changes in the coordinate difference can be explained by the change in the number of GPS satellites being tracked, which obviously affects the UAV ellipsoidal coordinates' performance.

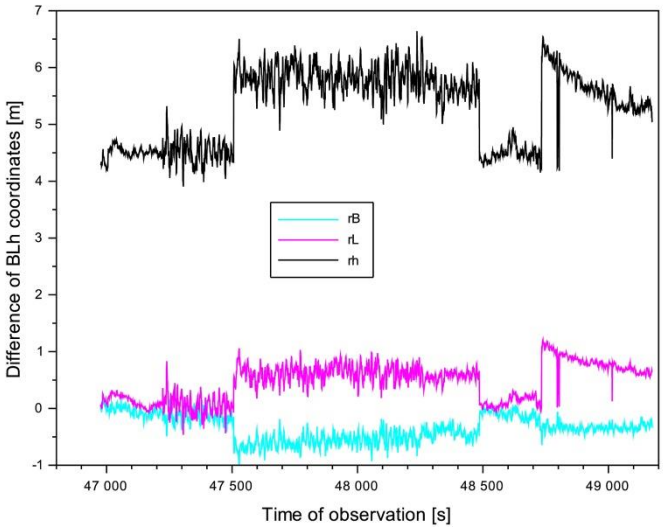

Figure 9. The difference of UAV coordinates between GPS+EGNOS solution and SPP.

6. Discussion

The discussion of the article will cover two main issues:

- analysis of the accuracy of the UAV positioning based on the proposed method against the SPP code solution without the use of EGNOS corrections,
- analysis of the results of the standard deviation based on the proposed method against the arithmetic mean model.

The major highlights in discussion will concerned to:

1. improvement the accuracy of UAV position based EGNOS solution;
2. improvement of the values of the standard deviation of BLh ellipsoidal coordinates based on the weighted mean model.

The first part of the discussion shows how the presented research method makes it possible to increase UAV positioning accuracy. For this purpose, two comparisons were presented. At first, the UAV coordinates based on GPS + EGNOS solution (Equations (1)–(5)) were compared in relation to the reference position determined by the RTK technique. At second, the GPS SPP solution (without EGNOS corrections) [48] were compared with RTK true trajectory.

Figure 10 shows the position error results along the B axis. The position error values along the B axis were calculated according to Equation(12). It should be noted that the DB position error results for the EGNOS solution are presented and analyzed in Figure 8. Figure 10 additionally shows position errors determined without the use of EGNOS corrections. It should be noted that the DB position errors without the use of EGNOS corrections range from +0.11 to +2.32 m. Additionally, the arithmetic mean is +1.21 m. Comparing both graphs, it can be seen that the EGNOS corrections significantly improved the accuracy of the UAV positioning for the B component. This increase in accuracy is as much as 29%.

Figure 11 shows the position error results along the L axis. The position error values along the L axis were calculated according to Equation (12). It should be noted that the DL position error results for the EGNOS solution are presented and analyzed in Figure 8. Figure 11 additionally shows position errors determined without the use of EGNOS corrections. It should be noted that the DL position errors without the use of EGNOS corrections range from -0.49 to +2.46 m. Additionally, the arithmetic mean is 1.02 m. Comparing both graphs, it can be seen that the EGNOS corrections significantly improved the accuracy of the UAV positioning for the L component. This increase in accuracy is around 46%.

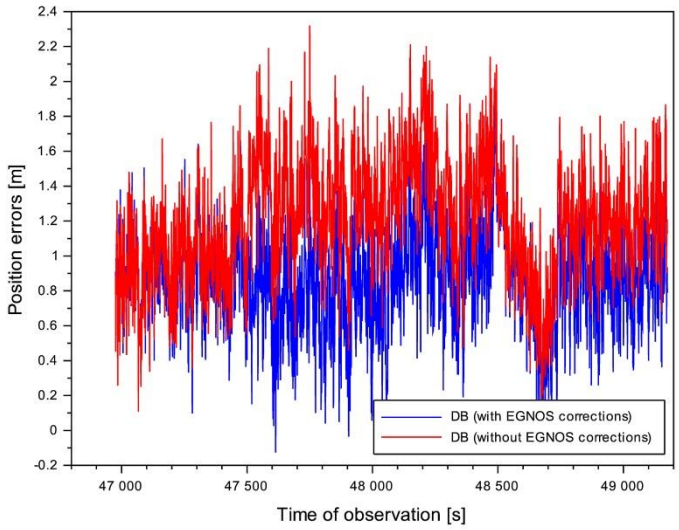

Figure 10. The results of position errors of the UAV with and without EGNOS corrections along the B axis.

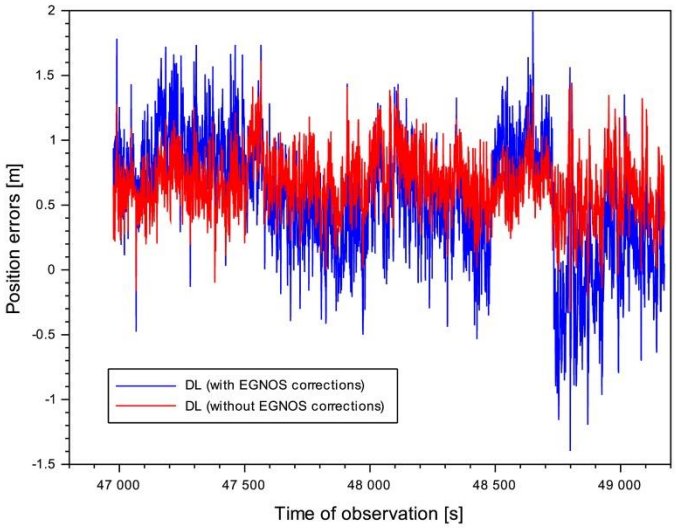

Figure 11. The results of position errors of the UAV with and without EGNOS corrections along the L axis.

Figure 12 shows the position error results along the h axis. The position error values along the Z axis were calculated according to Equation(12). It should be noted that the *Dh* position error results for the EGNOS solution are presented and analyzed in Figure 8. Figure 12 additionally shows position errors determined without the use of EGNOS corrections. It should be noted that the *Dh* position errors without the use of EGNOS corrections range from −7.59 to −1.28 m. Additionally, the arithmetic mean is −4.12 m. Comparing both graphs, it can be seen that the EGNOS corrections significantly improved the accuracy of the UAV positioning for the h component. This increase in accuracy is around 72%. Similar results were achieved as a result of research conducted by Dorn et al., 2017 [49]. In their work, the authors achieved the positioning accuracy for the SPP method for the 2D position of 1.090 m and the Z component (height) 2.140 m. Using the RTK solution allowed them to achieve accuracy for the 2D position of 0.255 m, while for the Z component (height) was 0.148 m.

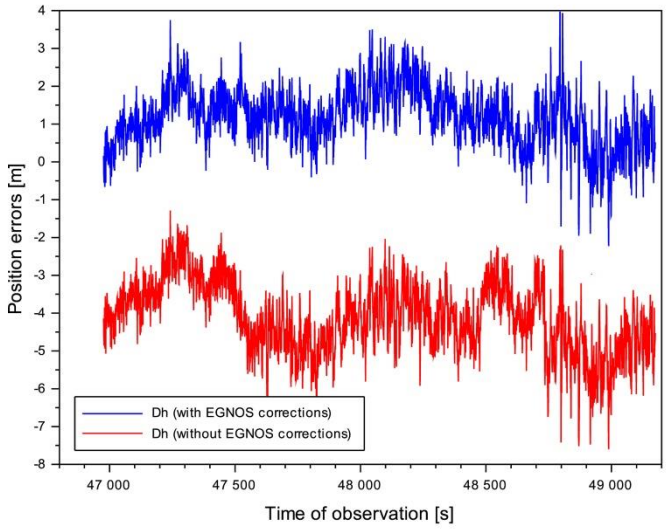

Figure 12. The results of position errors of the UAV with and without EGNOS corrections along the h axis.

Figure 12 shows a shift in the position error trend *Dh*. The mean value of the shift is about 5.3 m. The reason for this phenomenon depends mainly on the observation model. The observation model of the GPS + EGNOS solution shows the effect of long-term corrections for the position of the satellite and the satellite clock error and the ionospheric and tropospheric correction. It should be noted that the ellipsoidal height *h* and its accuracy *Dh* are dependent on the geometrical factor, i.e., the satellite-receiver position system. Mainly, the long-term corrections for the satellite position have a decisive influence on the performance of the vertical coordinate. It should not be forgotten that in GNSS measurements, the tropospheric correction, as one of the atmospheric corrections, also affects the ellipsoidal height value's determination. Summing up, the accuracy of ellipsoidal height determination is influenced by the long-term corrections for ephemeris data and the tropospheric correction for RTCA-MOPS model.

In the second part of the discussion, the authors presented the research analysis results concerning the comparison of the standard deviation value for the UAV position determination model based on the weighted mean and arithmetic mean methods. The mathematical scheme of determining the resultant UAV position using the arithmetic mean model can be written as below:

$$\begin{cases} B^m_{GPS/EGNOS} = \frac{B^i_{GPS/S123}+B^j_{GPS/S126}+B^k_{GPS/S136}}{i+j+k} \\ L^m_{GPS/EGNOS} = \frac{L^i_{GPS/S123}+L^j_{GPS/S126}+L^k_{GPS/S136}}{i+j+k} \\ h^m_{GPS/EGNOS} = \frac{h^i_{GPS/S123}+h^j_{GPS/S126}+h^k_{GPS/S136}}{i+j+k} \end{cases} \quad (17)$$

where: $i + j + k = 3$.

In turn, the values of the standard deviation from the weighted mean model can be determined as shown below:

$$\begin{cases} \delta B = \sqrt{\frac{v^2_{B,i}+v^2_{B,j}+v^2_{B,k}}{ns-1}} \\ \delta L = \sqrt{\frac{v^2_{L,i}+v^2_{L,j}+v^2_{L,k}}{ns-1}} \\ \delta h = \sqrt{\frac{v^2_{h,i}+v^2_{h,j}+v^2_{h,k}}{ns-1}} \end{cases} \quad (18)$$

Figure 13 shows the results of standard deviations δB determined from Equations (8) and (11). The δB parameter results for the weighted mean model are shown and described

in Figure 7. The maximum results of the δB parameter from the arithmetic mean model are equal to 0.64 m. The mean value of the δB parameter is 0.14 m. Comparing the plots it can be seen that the standard deviation values for the B component from the weighted mean model are smaller than for the arithmetic mean model. The improvement of the standard deviation results from the weighted mean model is about 21% compared to the arithmetic mean method.

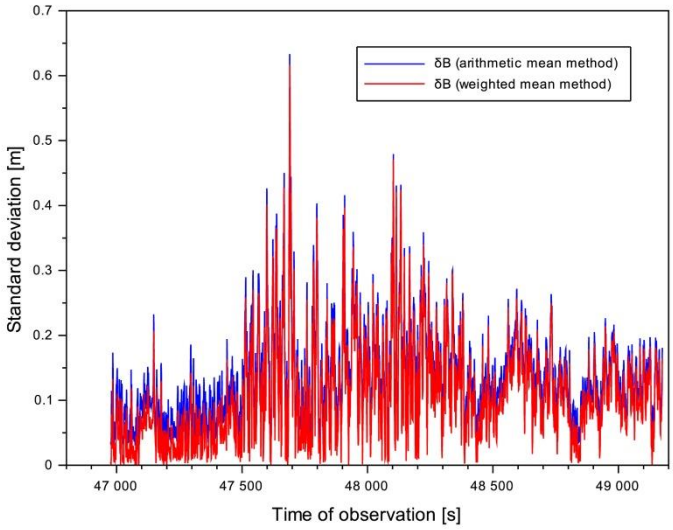

Figure 13. The comparison of standard deviations of the UAV along the B axis.

Figure 14 shows standard deviations δL determined from Equations (8) and (18). The δL parameter results for the weighted mean model are shown and described in Figure 7. The maximum results of the δL parameter from the arithmetic mean model are equal to 1.16 m. The mean value of the δL parameter is 0.27 m. Comparing the plots it can be seen that the standard deviation values for the L component from the weighted mean model are smaller than for the arithmetic mean model. The standard deviation results from the weighted mean model are about 26% higher than the arithmetic mean method.

Figure 15 shows the results of standard deviations δh determined from Equations (8) and (11). The δh parameter results for the weighted mean model are shown and described in Figure 7. The maximum results of the δh parameter from the arithmetic mean model are equal to 1.69 m. The mean value of the δh parameter is 0.26 m. Comparing the plots, it can be seen that the standard deviation values for the Z component from the weighted mean model are smaller than for the arithmetic mean model. The standard deviation results from the weighted mean model are about 50% higher than to the arithmetic mean method.

The research results presented in the discussion only show how important an element in the positioning and orientation in the UAV space is selecting an appropriate mathematical model for the description of the flight trajectory. Similar research work has been analyzed in other scientific articles. Thus, the work [50] shows a mathematical model for determining the UAV position in relation to the base station and the orientation of the UAV using the HPR rotation angles (Heading, Pitch, Roll). Additionally, the paper shows the error in determining the UAV position as a function of the distance from the base station and the errors of HPR rotation angles. The mathematical model shown in [50] has unique properties because it determines the positions and orientations of the UAV in relation to the base station. It can be said that the presented solution is a differential model of the position and orientation of the UAV.

This work shows how important the GNSS satellite technique is today. That is why more and more research works in the world concern the implementation of the GNSS sensor for precise positioning of the UAV. Therefore, in [51] a mathematical model for determining the position and orientation of an aircraft with the use of the single-frequency method for several onboard receivers is shown. Moreover, the paper defines the phase

uncertainty solution using the LAMBDA and C-LAMBDA methods for single-frequency receivers. Additionally, in work [51], the effectiveness of determining the orientation of the aircraft for relative GNSS positioning with the use of phase observations and ground reference stations was discussed. The accuracy of the aircraft orientation was set at 0.2°.

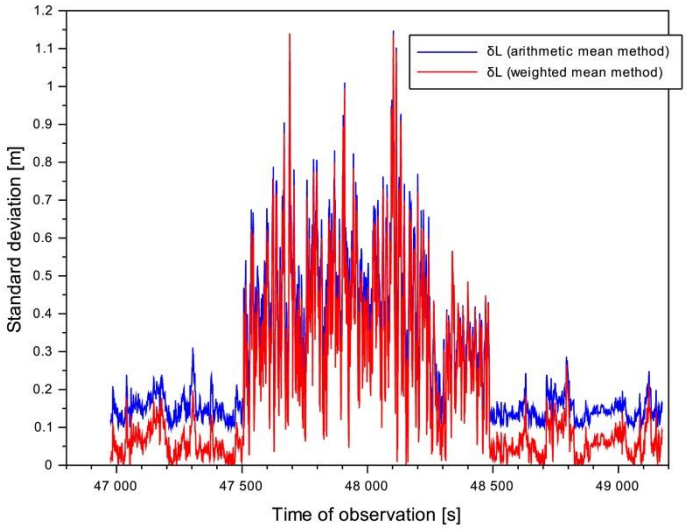

Figure 14. The comparison of standard deviations of the UAV along the L axis.

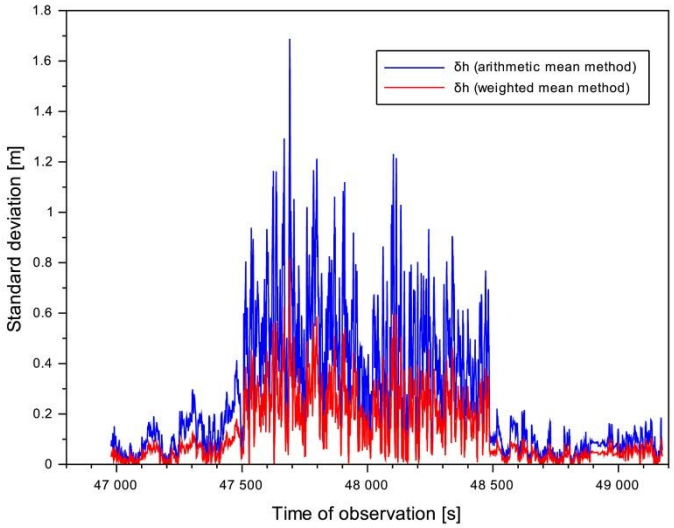

Figure 15. The comparison of standard deviations of the UAV along the h axis.

A very interesting approach in UAV positioning may be the PPP-RTK measurement technique [52]. The PPP-RTK method includes elements of PPP positioning, i.e., precise orbits and clocks as well as the characteristics of the phase center of the satellite antenna (or receiver) and the parameters of the atmosphere state from the RTK solution, i.e., the ZTD tropospheric delay model and the VTEC ionospheric delay determination model. Of course, in the case of the PPP-RTK solution, it is necessary to determine the Float phase's uncertainty. For UAV positioning, the PPP-RTK method will increase the accuracy of the determined coordinates to the level of cm ~ dm. It will also reduce orbit errors, tropospheric and ionospheric delays, and satellite clock errors in the PPP-RTK observation model. In UAV positioning, selecting an appropriate ionosphere and troposphere model is particularly important because the ionospheric correction shortens the vector between the reference station and the UAV position. In contrast, the tropospheric correction affects the

determination of the ellipsoidal height of the UAV. Thus, both atmospheric corrections are crucial here to improve the UAV's precise positioning performance.

7. Conclusions

The work concerns the development of a new resultant UAV position model based on the application of EGNOS corrections in GPS measurements. The paper presents the concept of determining the resultant UAV position on the basis of individual GPS/EGNOS solutions for the SPP code method. For this purpose, a weighted mean model was used to determine the ellipsoidal BLh coordinates of the UAV. The weighting of measurements considers the inverse of the square of the mean position error along the component axes of the BLh ellipsoidal frame. Accuracy measures in the form of position errors, the RMS error and the mean absolute error were determined for the computational strategy used. The new research method was tested to determine the position of the Tailsitter UAV.

On the basis of the performed tests, it was found that the mean values of the standard deviation of the BLh coordinates in the weighted mean model are better than 0.2 m. Moreover, the weighted mean model's use made it possible to increase the accuracy of the UAV position by about 29% for Latitude, 46% for Longitude and 72% for ellipsoidal height compared to the standard SPP positioning in the GPS receiver. It should be mentioned that the values of the standard deviation of the UAV position calculated from the weighted mean model improved by about 21 ÷ 50% compared to the solution from the arithmetic mean model. Such a significant improvement in accuracy in the weighted mean model only emphasizes the proposed solution's effectiveness. This research reinforces the thesis that the use of SBAS in UAV technology is necessary to improve the performance of GPS positioning on the L1 frequency. The authors plan to continue their work on the use of other augmentation systems such as SDCM or GAGAN in UAV technology in Poland.

Author Contributions: Conceptualization: K.K and D.W.; methodology: K.K.; validation, D.W. and K.K.; formal analysis, K.K.; investigation, K.K.; resources, K.K.; writing—original draft preparation, K.K. and D.W.; writing—review and editing, D.W.; visualization, K.K.; supervision, D.W.; project administration, D.W.; funding acquisition, D.W. All authors have read and agreed to the published version of the manuscript.

Funding: This research was funded by Military University of Technology, Faculty of Civil Engineering and Geodesy.

Institutional Review Board Statement: Not applicable.

Informed Consent Statement: Not applicable.

Data Availability Statement: Not applicable.

Acknowledgments: Many thanks to Michal Kedzierski from the Military University of Technology for his great help in acquiring UAV data.

Conflicts of Interest: The authors declare no conflict of interest.

References

1. Wierzbicki, D.; Krasuski, K. Methods of Predicting the Heading, Pitch and Roll Angles for an Unmanned Aerial Vehicle. *Commun. Sci. Lett. Univ. Zilina* **2020**, *22*, 52–59. [CrossRef]
2. Wierzbicki, D.; Krasuski, K. Determining the Elements of Exterior Orientation in Aerial Triangulation Processing Using UAV Technology. *Commun. Sci. Lett. Univ. Zilina* **2020**, *22*, 15–24. [CrossRef]
3. Lalak, M.; Wierzbicki, D.; Kędzierski, M. Methodology of Processing Single-Strip Blocks of Imagery with Reduction and Optimization Number of Ground Control Points in UAV Photogrammetry. *Remote. Sens.* **2020**, *12*, 3336. [CrossRef]
4. Wierzbicki, D.; Krasuski, K. Determination the coordinates of the projection center in the digital aerial triangulation using data from Unmanned Aerial Vehicle. *Aparatura Badawcza i Dydaktyczna* **2016**, *3*, 127–134. (In Polish)
5. Wang, S.; Zhan, X.; Zhai, Y.; Chi, C.; Shen, J. Highly reliable relative navigation for multi-UAV formation flight in urban environments. *Chin. J. Aeronaut.* **2020**. [CrossRef]
6. Sanz Subirana, J.; Juan Zornoza, J.M.; Hernandez-Pajares, M. Fundamentals and algorithms. In *GNSS Data Processing*; ESA Communications ESTEC: Noordwijk, The Netherlands, 2013; Volume 1, ISBN 978-92-9221-886-7.
7. Xu, G. *GPS: Theory, Algorithms and Applications*; Springer: Berlin/Heidelberg, Geramny, 2007; p. 340, ISBN 978-3-540-72715-6.

8. Hofmann-Wellenhof, B.; Lichtenegger, H.; Collins, J. *Global Positioning System Theory and Practice*, 5th ed.; Springer: Berlin/Heidelberg, Geramny, 2001.
9. Yoon, H.; Seok, H.; Lim, C.; Park, B. An Online SBAS Service to Improve Drone Navigation Performance in High-Elevation Masked Areas. *Sensors* **2020**, *20*, 3047. [CrossRef]
10. Grunwald, G.; Ciećko, A.; Krasuski, K.; Kaźmierczak, R. The GPS/EGNOS Positioning Quality in APV-1 and LPV-200 flight procedures. *Commun. Sci. Lett. Univ. Zilina* **2021**, *23*, E23–E34. [CrossRef]
11. Ciećko, A.; Grunwald, G. Klobuchar, NeQuick G, and EGNOS Ionospheric Models for GPS/EGNOS Single-Frequency Positioning under 6–12 September 2017 Space Weather Events. *Appl. Sci.* **2020**, *10*, 1553. [CrossRef]
12. Dorn, M.; Lesjak, R.; Huber, K.; Wieser, M. Improvement of the GNSS Solution for Advanced RPAS Applications Utilizing PPp RTK or Sensor Integration. In Proceedings of the International Micro Air Vehicle Conference and Flight Competition (IMAV), Aachen, Germany, 15–18 September 2015; Volume 15. No. 18.
13. *EGNOS Safety of Life (SoL) Service Definition Document (v. 3.1)*; The European GNSS Agency (GSA): Prague, Czech Republic, 2016.
14. Ciećko, A.; Bakuła, M.; Grunwald, G.; Ćwiklak, J. Examination of Multi-Receiver GPS/EGNOS Positioning with Kalman Filtering and Validation Based on CORS Stations. *Sensors* **2020**, *20*, 2732. [CrossRef]
15. Grunwald, G.; Bakuła, M.; Ciećko, A.; Kaźmierczak, R. Examination of GPS/EGNOS integrity in north-eastern Poland. *IET Radar Sonar Navig.* **2016**, *10*, 114–121. [CrossRef]
16. Ciećko, A. Analysis of the EGNOS quality parameters during high ionosphere activity. *IET Radar Sonar Navig.* **2019**, *13*, 1131–1139. [CrossRef]
17. European GNSS Agency (GSA). *EGNOS Safety of Life (SoL) Service Definition Document (v. 3.3)*; The European GNSS Agency: Prague, Czech Republic, 2019.
18. Balsi, M.; Prem, S.; Williame, K.; Teboul, D.; Délétraz, L.; Hebrard Capdeville, P.I. Establishing new foundations for the use of remotely-piloted aircraft systems for civilian applications. *Int. Arch. Photogramm. Remote Sens. Spatial Inf. Sci.* **2019**, *2*, 197–201. [CrossRef]
19. European GNSS Agency. GNSS Market Report. Available online: https://www.gsa.europa.eu/system/files/reports/market_report_issue_6_v2.pdf (accessed on 22 July 2020).
20. Alarcón, F.; Viguria, A.; Vilardaga, S.; Montolio, J.; Soley, S. EGNOS-based Navigation and Surveillance System to Support the Approval of RPAS Operations. In Proceedings of the 9th SESAR Innovation Days, Athens, Greece, 2–6 December 2019.
21. Sheridan, I. Drones and global navigation satellite systems: Current evidence from polar scientists. *R. Soc. Open Sci.* **2020**, *7*, 191494. [CrossRef] [PubMed]
22. European GNSS Agency (GSA). European Global Navigation Satellit Systems (EGNSS) for Drones Operations. Available online: https://op.europa.eu/en/publication-detail/-/publication/03e63719-5784-11ea-8b81-01aa75ed71a1 (accessed on 22 July 2020).
23. Tamouridou, A.A.; Alexandridis, T.; Pantazi, X.; Lagopodi, A.L.; Kashefi, J.; Kasampalis, D.A.; Kontouris, G.; Moshou, D. Application of Multilayer Perceptron with Automatic Relevance Determination on Weed Mapping Using UAV Multispectral Imagery. *Sensors* **2017**, *17*, 2307. [CrossRef] [PubMed]
24. Molina, P.; Colomina, I.; Vitoria, T.; Silva, P.F.; Stebler, Y.; Skaloud, J.; Kornus, W.; Prades, R. EGNOS-based multi-sensor accurate and reliable navigation. *ISPRS Int. Arch. Photogramm. Remote. Sens. Spat. Inf. Sci.* **2012**, *1*, 87–93. [CrossRef]
25. Molina, P.; Colomina, I.; Vitoria, T.; Freire, P.; Skaloud, J.; Kornus, W.; Mata, R.; Aguilera, C. The CLOSE-SEARCH project UAV-based search operations using thermal imaging and EGNOS-SoL navigation. In Proceedings of the GeoInformation for Disaster Management conference (Gi4DM 2011), Antalya, Turkey, 3–7 May 2011.
26. Molina, P.; Colomina, I.; Victoria, T.; Skaloud, J.; Kornus, W.; Prades, R.; Aguilera, C. Searching lost people with UAVS: The system and results of the CLOSE-SEARCH project. *Int. Arch. Photogramm. Remote Sens. Spat. Inf. Sci.* **2012**, *39*, 441–446. [CrossRef]
27. Molina, P.; Colomina, I.; Vitoria, T.; Silva, P.F.; Bandeiras, J.; Stebler, Y.; Skaloud, J.; Kornus, W.; Prades, R.; Aguilera, C. Integrity Aspects of Hybrid EGNOS-based Navigation on Support of Search-And-Rescue Missions with UAVs. In Proceedings of the 24th International Technical Meeting of the Satellite Division of The Institute of Navigation (ION GNSS 2011), Portland, OR, USA, 20–23 September 2011; pp. 3773–3781.
28. Fellner, A.; Sulkowski, J.; Trominski, P.; Zadrag, P. The use of reference systems for UAV flight routing. In Proceedings of the EGU General Assembly, Vienna, Austria, 22–27 April 2012; p. 6434.
29. Pullen, S.; Enge, P.; Lee, J. Local-Area Differential GNSS Architectures Optimized to Support Unmanned Aerial Vehicles (UAVs). In Proceedings of the International Technical Meeting of the Institute of Navigation (ION ITM 2013), San Diego, CA, USA, 28–30 January 2013; pp. 559–571.
30. Watanabe, Y.; Manecy, A.; Hiba, A.; Nagai, S.; Shin, A. Vision-integrated navigation system for aircraft final approach in case of GNSS/SBAS or ILS failures. In Proceedings of the AIAA Scitech 2019, San Diego, CA, USA, 7–11 January 2009; p. 113. [CrossRef]
31. Geister, R.; Limmer, L.; Rippl, M.; Dautermann, T. Total system error performance of drones for an unmanned PBN concept. Presented at the IEEE Integrated Communications, Navigation, Surveillance Conference (ICNS 2018). Herndon, VA, USA, 10–12 April 2018; pp. 2D4-1–2D4-9. [CrossRef]
32. Krasuski, K.; Wierzbicki, D. Monitoring Aircraft Position Using EGNOS Data for the SBAS APV Approach to the Landing Procedure. *Sensors* **2020**, *20*, 1945. [CrossRef]
33. Ibáñez Segura, D.; Rovira Garcia, A.; Alonso, M.T.; Sanz, J.; Juan, J.M.; González Casado, G.; López Martínez, M. EGNOS 1046 Maritime Service Assessment. *Sensors* **2020**, *20*, 276. [CrossRef]

34. Jan, S.-S. Vertical Guidance Performance Analysis of the L1-L5 Dual-Frequency GPS/WAAS User Avionics Sensor. *Sensors* **2010**, *10*, 2609–2625. [CrossRef]
35. Krasuski, K. The Research of Accuracy of Aircraft Position Using SPP Code Method. Ph.D. Thesis, Warsaw University of Technology, Warsaw, Poland, 2019; pp. 1–106. (In Polish).
36. Krasuski, K.; Ćwiklak, J.; Grzegorzewski, M. Aircraft positioning using GPS/GLONASS code observations. *Aircr. Eng. Aerosp. Technol.* **2019**, *92*, 163–171. [CrossRef]
37. Osada, E. *Geodesy*; Oficyna Wydawnicza Politechniki Wroclawskiej: Wroclaw, Poland, 2001; Volume 92, pp. 236–241, ISBN 83-7085-663-2. (In Polish)
38. Krasuski, K.; Ciećko, A.; Bakuła, M.; Wierzbicki, D. New Strategy for Improving the Accuracy of Aircraft Positioning Based on GPS SPP Solution. *Sensors* **2020**, *20*, 4921. [CrossRef]
39. Przestrzelski, P.; Bakuła, M.; Galas, R. The integrated use of GPS/GLONASS observations in network code differential positioning. *GPS Solut.* **2017**, *21*, 627–638. [CrossRef]
40. Krasuski, K.; Savchuk, S. Accuracy Assessment of Aircraft Positioning Using the Dual-Frequency GPS Code Observations in Aviation. *Commun. Sci. Lett. Univ. Zilina* **2020**, *22*, 23–30. [CrossRef]
41. SBAS Mentor Website. Available online: http://www.egnos-pro.esa.int/sbasmentor/index.html (accessed on 30 August 2020).
42. Takasu, T. RTKLIB ver. 2.4.2 Manual, RTKLIB: An Open Source Program. Package for GNSS Positioning. 2013. Available online: http://www.rtklib.com/prog/manual_2.4.2.pdf (accessed on 30 August 2020).
43. Jafernik, H.; Krasuski, K.; Ćwiklak, J. Tests of the EGNOS System for Recovery of Aircraft Position in Civil Aircraft Transport. *Revista Europea de Derecho de la Navegación Marítima y Aeronáutica*. No. 36. 2019, pp. 17–38. Available online: https://dialnet.unirioja.es/servlet/articulo?codigo=7387174 (accessed on 30 January 2021).
44. Scilab Website. Available online: https://www.scilab.org/ (accessed on 30 August 2020).
45. Felski, A.; Nowak, A. Accuracy and availability of EGNOS—Results of observations. *Artif. Satell.* **2011**, *46*, 111–118. [CrossRef]
46. Jafernik, H. Assessment of the Usefulness of EGNOS Differential Corrections in Conducting GPS Static Measurements. *Int. J. Eng. Res. Appl.* **2016**, *6*, 25–30.
47. Kozuba, J.; Krasuski, K.; Ćwiklak, J.; Jafernik, H. Aircraft position determination in SBAS system in air transport. In Proceedings of the 17th International Conference Engineering for rural development, Jelgava, Latvia, 23–25 May 2018; pp. 788–794. [CrossRef]
48. Tian, A.; Dong, D.; Ning, D.; Fu, C. GPS Single Point Positioning Algorithm Based on Least Squares. In Proceedings of the 6th International Symposium on Computational Intelligence and Design, Hangzhou, China, 28–29 October 2013; pp. 16–19. [CrossRef]
49. Dorn, M.; Filwarny, J.O.; Wieser, M. Inertially-aided RTK based on tightly-coupled integration using low-cost GNSS receivers. In Proceedings of the 2017 European Navigation Conference (ENC), Geneva, Switzerland, 9–12 May 2017; IEEE: Piscataway, NJ, USA, 2017; pp. 186–197.
50. Marinho, M.A.; Ferreira, R.S.J.; da Costa, J.P.C.; de Freitas, E.P.; Antreich, F.; Liu, K.; So, H.C.; Rafael, T.; Zelenovsky, R. Antenna array based positioning scheme for unmanned aerial vehicles. In Proceedings of the 17th International ITG Workshop on Smart Antennas (WSA 2013), Stuttgart, Germany, 13–14 March 2013; pp. 1–6.
51. Teunissen, P.J.G.; Giorgi, G.; Buist, P.J. Testing of a new single-frequency GNSS carrier phase attitude determination method: Land, ship and aircraft experiments. *GPS Solut.* **2011**, *15*, 15–28. [CrossRef]
52. Ma, H.; Zhao, Q.; Verhagen, S.; Psychas, D.; Liu, X. Assessing the Performance of Multi-GNSS PPP-RTK in the Local Area. *Remote Sens.* **2020**, *12*, 3343. [CrossRef]